ACS Macro Letters

Letter

pubs.acs.org/macroletters

Determination of Local Packing Structure of Mesomorphic Form of Isotactic Polypropylene by Solid-State NMR

Shichen Yuan,[†] Zhen Li,[†] Jia Kang,[†] You-lee Hong,[†] Akihiro Kamimura,[‡] Akihiro Otsubo,[‡] and Toshikazu Miyoshi*,[†]

[†]Department of Polymer Science, The University of Akron, Akron, Ohio 44325-3909, United States

[‡]SunAllomer, Ltd., 3-2 Yako 2-chome, Kawasaki-ku Kawasaki 210-0863, Japan

Supporting Information

ABSTRACT: Understanding the local packing structures of a disordered mesomorphic phase is a challenging issue in polymer characterization. In this work, $^{13}C-^{13}C$ through-space interactions, as well as a molecular dynamics analysis based on the reorientation of chemical shift anisotropy (CSA), were proposed for the evaluation of the local packing structure of the mesomorphic form of isotactic polypropylene (*i*PP). $^{13}C-^{13}C$ double quantum (DQ) buildup curves of ^{13}C 15% CH_3 selectively labeled *i*PP and spin-dynamics simulations demonstrated that the local packing structures in the mesomorphic form were very similar to the packing in the β phase. Moreover, centerband only detection of exchange (CODEX) NMR proved that the correlation time $\langle\tau_c\rangle$ of the overall stem dynamics in the mesomorphic form followed the same Arrhenius line observed for the β phase, but it deviated from that for the α phase. Based on both structural and dynamic results, it was concluded that the local packing structure in the mesomorphic form was exceedingly close or the same as that of the β phase.

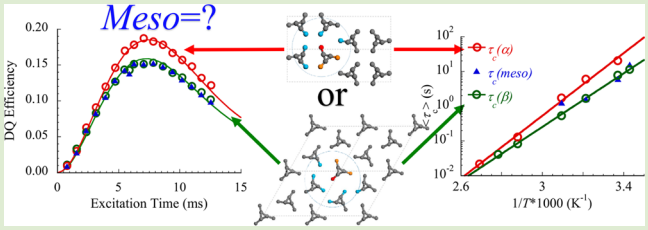

A mesomorphic form is an intermediate state between ordered crystals and disordered liquids. Under rapid quenching from the melt state or slow crystallization from the glassy state, or through certain processing, such a unique form can often be observed in semicrystalline polymers. A mesomorphic form features various types of structural defects and does not possess three-dimensional long-range order. Thus, conducting detailed local structural analysis of a mesomorphic form remains a challenging issue in polymer characterization.

Isotactic polypropylene (*i*PP) is an important semicrystalline material in both the industrial and the academic realms. When an *i*PP melt without a specific nucleation agent is cooled, the stable α phase is formed. Rapid quenching by supercooling at rates above ~90 K/s leads to the formation of the mesomorphic form.[1] Mesomorphic *i*PP was first proposed by Natta et al.[2] To date, various models, including those characterized as a smectic bundle,[3] α phase,[4] β phase,[5] conformationally disordered (CONDIS) crystals,[6] and a mixture of α and β characters,[7,8] have been proposed as local packing structures for the mesomorphic form. These models are based on observations of XRD patterns, which simply yield two very broad maxima at 2θ = 15.1° and 21.7°, as shown in Figure S1. An alternative tool is high-resolution ^{13}C NMR, which is sensitive to local conformations and packing structures of polymers. In the case of *i*PP crystals, however, chemical shifts and line shapes of the mesomorphic form are very similar to those of the α and β phases (Figure S2). Among the various studies conducted in this context, two have provided evidence supporting the real mesomorphic form structures of *i*PP. Gomez et al.[9] used the ^{13}C spin–lattice relaxation time (T_1) of the methyl group, which is empirically known to be sensitive to local packing structure. The similarity of the T_1 values between the mesomorphic and β phases supports the fact that the packing structure of the mesomorphic form resembles that of the β phase. Alternatively, Corradini et al.[7,8]measured XRD patterns for the stretched mesomorphic form at stretching ratios of up to 600% and calculated the diffraction patterns based on the various packing models. The authors rejected the assumption that the mesomorphic form is composed of only the α or β phase and proposed a mixed structure of the two phases in which the averaged interstem distance is approximately 6.0 Å, shorter than the distance in the β phase (6.3 Å) and longer than the average distance in the α phase (5.8 Å). They also pointed out that correlations of stems in the mesomorphic form are lost at distances longer than 4 nm.

To correctly understand the local packing structures of the mesomorphic structure, a novel strategy that can selectively access the short-range correlation between the closest stems at lengths less than ~1 nm is necessary. In solid-state NMR spectroscopy, magnetically anisotropic interactions, such as chemical shift anisotropy (CSA) and dipolar interactions, can provide detailed information regarding orientations,[10] conformations,[11] packing structures,[12,13] intermolecular interactions,[14,15] and molecular dynamics of polymers at the atomic

Received: December 12, 2014
Accepted: January 8, 2015
Published: January 9, 2015

DOI: 10.1021/mz5007969
ACS Macro Lett. 2015, 4, 143–146

scale.[16] Very recently, we proposed a novel approach using $^{13}C-^{13}C$ double quantum (DQ) NMR combined with selectively ^{13}C isotropic labeling to investigate the chain trajectory of polymers in melt- and solution-grown crystals, in which interstem $^{13}C-^{13}C$ dipolar interactions were utilized.[17,18] This strategy might be useful in characterizing the packing structures of even highly disordered mesomorphic forms. Besides, the molecular dynamics of chains are highly dependent on the available dynamic spaces. Thus, the kinetics and geometries of molecular motion are highly dependent on the packing structures, that is, a crystalline lattice with three-dimensional order limits molecular motions to discrete jump motions of the crystalline stems.[16,19]

In this study, we investigated the local packing structure of the mesomorphic form of *i*PP using $^{13}C-^{13}C$ DQ and centerband only detection of exchange (CODEX)[20] NMR. In all experiments, a spin−lattice relaxation time filter ($T_{1\rho H}$) was incorporated into the pulse programs to suppress the amorphous contributions to the NMR spectra (see details in the experimental section in the SI and Figure S3).

Figures 1a and 2a depict the ^{13}C single quantum (SQ) and DQ NMR spectra of 15% $^{13}CH_3$ labeled *i*PP in the α and β

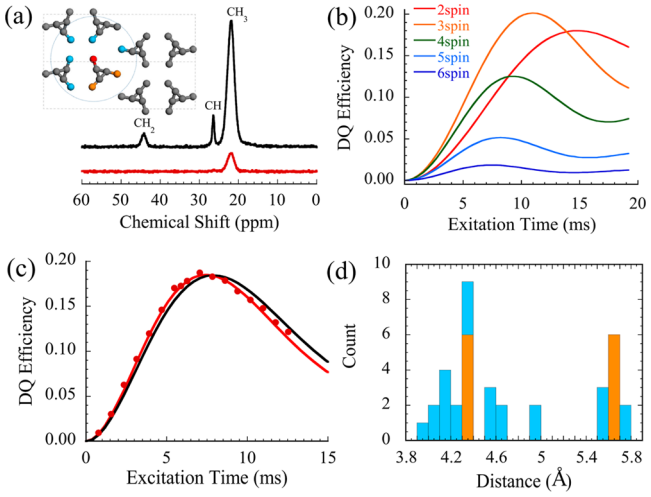

Figure 1. (a) ^{13}C $T_{1\rho H}$ filtered DQ (red) and SQ (black) CPMAS NMR spectra of 15% $^{13}CH_3$-labeled α *i*PP measured at 298 K. The inset shows a top view of the α packing structure. The methyl groups shown in red and different colors (light blue (interstem) and orange (intrastem)) indicate the detected and surrounding carbons within 6 Å. (b) Simulated DQ sub-buildup curves for the observation spin in (a), (c) $^{13}C-^{13}C$ DQ buildup curves of the $^{13}CH_3$ integral in α-*i*PP samples (red filled circle). The black and red curves are the simulated curves for the 100% and 98% shrink α models, respectively. (d) Distribution of the distances between the observation spins and the surrounding spins in the α phase (orange (intrastem) and light blue (interstem)).

phases, respectively, at 298 K (see the NMR experiments in SI). The latter was obtained using an excitation time (τ_{ex}) of 5.9 ms. DQ NMR generates only the CH_3 signals due to $^{13}C-^{13}C$ dipolar interactions. For the α phase, the DQ efficiency ξ is 0.17, where ξ was obtained by the integration ratios of the DQ to the SQ signals. Figures 1c and 2c show the experimentally obtained DQ buildup curves of ^{13}C labeled α and β *i*PP, respectively, as a function of τ_{ex}. The former and the latter show maximum ξ values of 0.19 at τ_{ex} = 7.0 ms and 0.15 at τ_{ex} = 7.8 ms, respectively. Different buildup curves indicate that DQ

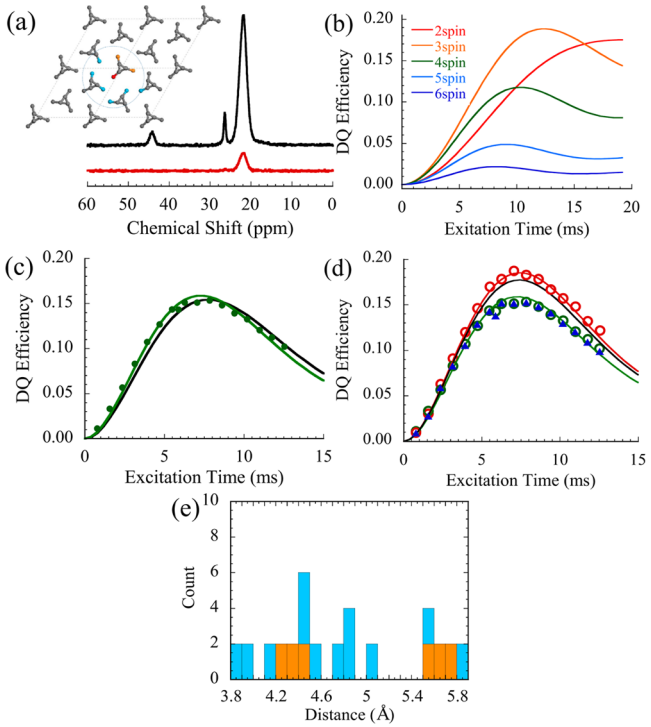

Figure 2. (a) ^{13}C $T_{1\rho H}$ filtered DQ (red) and SQ (black) CPMAS NMR spectra of 15% $^{13}CH_3$-labeled β *i*PP measured at 298 K. The inset shows a top view of the β packing structure, and the color scheme is the same as that of Figure 1a. (b) Simulated DQ sub-buildup curves for the observation spin in (a). (c) $^{13}C-^{13}C$ DQ buildup curves of the $^{13}CH_3$ signal in the β samples (green filled circle). The black and red curves show simulated curves for the 100% and 98% shrink β models, respectively. (d) DQ buildup curves of α (red open circle), β (green open circle), and mesomorphic *i*PP samples (blue filled triangle). The red and green curves are the best-fit buildup curves duplicated from Figure 1c and (c), respectively, and the black curve is a mixed curve of the best-fit DQ curves for α and β packing in a ratio of 7:3, respectively. (e) Distribution of the distances between the observed spins and the neighboring labeled spins in the β phase ((orange (intrastem) and light blue (interstem)).

NMR based on $^{13}CH_3-^{13}CH_3$ dipolar interactions can discern the local packing structure between the α and β phases.

Figures 1a and 2a show the packing structures of the α (monoclinic lattice with a = 6.6 ± 0.1 Å, b = 20.8 ± 0.1 Å, and c = 6.5 ± 0.1 Å, β = 99.5°)[21] and the β (trigonal lattice with $a = b$ = 11.0 ± 0.1 Å and c = 6.5 ± 0.1 Å, γ = 120°)[22] phases, where the colored CH_3 carbons were labeled by ^{13}C. To simulate the DQ buildup curves, we considered 13 spin systems: one reference spin and 12 surrounding spins. The model system consisted of a reference methyl carbon (colored by red) plus the 12 closest surrounding carbons (interstem and intrastem shown in light blue and orange, respectively) at a distance less than 6 Å (insets in Figures 1a and 2a). The apparent ξ at a single site shown in red in Figures 1a and 2a can be defined by the relation $\xi(\tau_{eq}) = \sum_{m=1}^{13} a_m(\tau_{eq}) \exp(-\tau_{eq}/T_2)$,[18] where the term $a_m(\tau_{eq})$ is the ideal DQ efficiency based on the interacting spins, the internuclear distances and the spin topologies in the ^{13}C spin systems that were determined by the crystal unit cell; the term T_2 is the incoherent relaxation, which in principle includes unwanted contributions from the CSA, insufficient decoupling, an rf. imperfection, and long-range dipolar interactions at lengths >6 Å that are not treated in the simulations. The 15% labeling ratio of the methyl groups

DOI: 10.1021/mz5007969
ACS Macro Lett. 2015, 4, 143−146

statistically produces different spin systems among the 13 sites, resulting in different build-up curves. In these m-spin systems, $a_m(\tau_{eq})$ is expressed as $a_m(\tau_{eq}) = (\Sigma w_{m\_j} q_{m\_j}(\tau_{eq}))\ P_m$, where $q_{m\_j}(\tau_{eq})$ is an individual simulated curve for the m-spin systems, j is the spin topology of a given m-spin system, and w_{m_j} is the probability of a given m-spin system with spin topology j ($\sum_{m=1}^{13} w_{m\_j} = 1$). P_m represents the probability of finding m spins among the 13 sites and is calculated using the equations $P_m = C_{m-1}^{12}(x)(1-x)^{12-(m-1)}$ and $\sum_{m=1}^{13} P_m = 1$ (see details in Table S1), where C_{m-1}^{12} and x are the combination and isotope labeling ratios, respectively. For spin numbers equal to or greater than 7, $\sum_{m=7}^{13} P_m$ was only ~0.5%, and the DQ curve for the six-spin system was nearly identical to that for the seven-spin system. Thus, the DQ curves for interactions involving more than seven spins were assumed to be the same as those for the six-spin system. The DQ build-up curves corresponding to $a_m\ (\tau_{eq})\ P_m$ are depicted in Figures 1b and 2b. In the α model, three types of methyl groups located in the same 3_1 helices (in the β model, three types also exist but each of them is located in one of three helices in one unit cell), and the ideal buildup curves for α (β) were obtained by averaging the DQ buildup curves for all three cases. All of the possible spin interactions with an apparent exponential T_2 of 9.0 ± 1.0 (α) and 8.0 ± 1.0 ms (β) resulted in one simulated DQ curve (the black curves in Figures 1c and 2c). Both calculated curves showed a slightly slower buildup than the experimental curves. Therefore, the simulated DQ curves with 2% shorter internuclear distances compared to the original distances in both the α and β phases and an apparent T_2 value of 8.5 ± 1.0 (α) and 7.6 ± 1.0 ms (β) could reproduce the experimental results. The best-fit curves are drawn as red and green curves in Figures 1c and 2c, respectively. The distributions of the 36 $^{13}CH_3-^{13}CH_3$ distances in the α and β models are summarized in Figures 1d and 2e, respectively, where 36 distances indicate 12 distances multiplied by 3 sites. The interchain $^{13}CH_3-^{13}CH_3$ distances less than 4.4 Å (average) yield 40% of the 24 $^{13}CH_3-^{13}CH_3$ distances in the α phase and 20% in the β phase. The difference in the distance distributions is consistent with the fact that the packing structure of the racemic α crystals is denser than the chiral β ones. These structural differences result in faster and higher DQ efficiencies in the α phase compare with those in the β phase. The optimized fitting curves provide interstem distances of 5.7 and 6.2 Å for the α and β phases, respectively.

Figure 2d shows the $^{13}C-^{13}C$ DQ buildup curve of the mesomorphic form (filled blue triangles) with maximum ξ value of 0.15 at τ_{ex} = 7.8 ms. Surprisingly, the DQ curve completely overlaps with the calculated (green) and experimental β curves (green open circle), which were much lower than the α curve (red). This experimental result clearly invalidates the α phase as a relevant model. Corradini et al. reported that the mesomorphic form consisted of mixed crystals of α and β lattices and that the dominant component was monoclinic (approximately 70%).[8] This intermediate state is simply approximated in terms of a mixed curve of the best-fit α and β curves with a ratio of 7:3, respectively (black in Figure 2d). A DQ curve higher than the experimental curve would invalidate the mixed model. The DQ experiment reveals that the local environment for the mesophase with stem−stem distance of 6.2 Å is very close or the same as that for the β phase.

Figure 3a shows the CODEX exchange and reference spectra for the mesomorphic form with a mixing time t_{mix} of 1 s at 310 K.

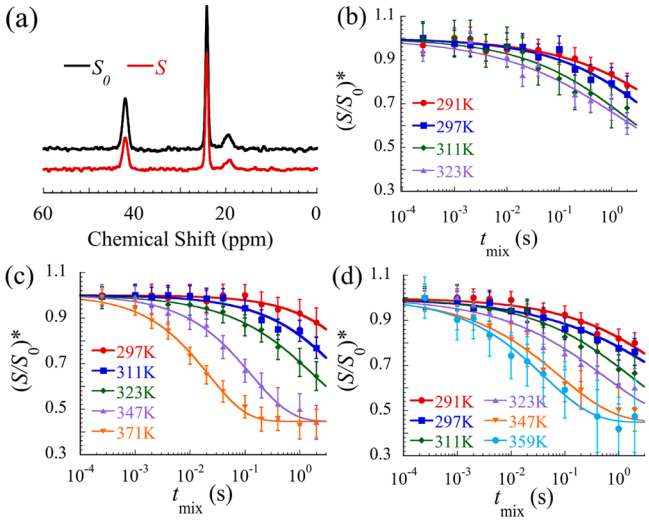

Figure 3. (a) $T_{1\rho H}$ filtered CODEX exchange (S) and reference (S_0) spectra of the mesomorphic sample at 310 K. (b−d) t_{mix} dependence of the CODEX $(S/S_0)^*$ intensity ratios for the CH_2 signals for the (b) mesomorphic, (c) α, and (d) β *i*PP at various temperatures.

Within a dynamic window of 1 s, segments of the mesomorphic form change orientations relative to the magnetic field. Therefore, the S spectrum results in lower intensities than those for S_0.

Indeed, CODEX decaying curve at a long mixing time of the second order includes additional spin exchange effects due to spin diffusion even in natural abundance.[23] Thus, a detailed analysis requires a correction for spin diffusion. Figure 3b demonstrates the t_{mix} dependence of the CODEX $(S/S_0)^*$ decay curves for the CH_2 signals in the mesomorphic sample at temperatures up to 323 K, where * indicates the pure decay dynamics after the spin-diffusion correction. To analyze the kinetic parameters of the dynamics, curve fitting to the experimental data was accomplished using the following empirical equation:[20]

$$(S/S_0(t_{mix}))^* = 1 - a(1 - \exp(-(t_m/\langle\tau_c\rangle)^\beta)) \quad (1)$$

where a is defined by p (available dynamics sites) as $a = (p-1)/p$ and β is the distribution parameter ($0 < \beta \leq 1$). For the α and β samples, the temperature dependence of CODEX t_{mix} decay curves is shown in Figures 3c and 3d, respectively. Thermally activated molecular dynamics in both the α and β phases clearly induced plateau values of ~0.45 at 371 and 359 K, respectively. Unfortunately, we could not observe a plateau for the mesomorphic form due to a phase transition to the α phase above 323 K. We thereby applied a = 0.55 to analyze the dynamics of all three forms at low temperatures at which a plateau was not obtained. Using eq 1, the best-fit curves were plotted as shown in Figure 3b−d, and the best-fit parameters are listed in Table S2.

Figure 4 shows the Arrhenius plots of $\langle\tau_c\rangle$ in all three forms. As shown in Figure 4, the activation energies were estimated to be E_a = 86.3 kJ/mol for the α phase and E_a = 74.3 kJ/mol for the β phase. The obtained E_a and $\langle\tau_c\rangle$ values are reasonably explained in terms of the slightly different packing structures of

DOI: 10.1021/mz5007969
ACS Macro Lett. 2015, 4, 143−146

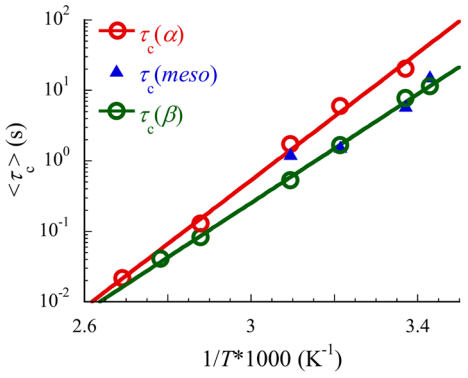

Figure 4. Arrhenius plots of $\langle\tau_c\rangle$ for the large-amplitude motions of the stems in the α (red open circle), β (green open circle), and mesomorphic forms (blue filled triangle).

the α (stem−stem distance of 5.7 Å) and β phases (6.2 Å), respectively. For the mesomorphic form, the experimental temperature window was limited due to the meso-α transition. The temperature dependence of the $\langle\tau_c\rangle$ values in the mesomorphic samples at temperatures up to 311 K completely followed the Arrhenius line for the β phase and largely deviated from that of the α phase. This dynamics result also invalidates the notion that the local packing structures of the mesomorphic form are composed of the α phase or are mixtures of the two crystals and supports the affiliation with the β phase. To date, we have not examined CONDIS crystals proposed by Wunderlich,[6] which possess a lower density (looser packing) and faster dynamics than those for the ordered crystals.[6,24] Both local packing structures evaluated by DQ and the dynamics results obtained by CODEX reasonably reject the CONDIS crystal as a relevant structure for the mesomorphic form. Very recently, Yamamoto performed MD simulations on the strain-induced crystallization of *i*PP oligomers (50 repeat units).[25] MD simulations detected a hexagonal form consisting of mixed right- and left-hand helices. Unfortunately, their calculated snapshots included an enormous number of atomic coordinates for the CH_3 groups of the stems that possessed different packing structures. Thereby, DQ buildup simulations were not realized. Notably, the difference between hexagonal and trigonal packing is quite minor.

In summary, combined experiments of local packing and dynamic analyses based on $^{13}C-^{13}C$ interstem dipolar interactions and CSA reorientations, respectively, provided detailed local packing structures of the mesomorphic form of *i*PP for the first time. It was concluded that the structures of the mesomorphic form are exceedingly similar to those of the trigonal β phase; this finding supports the early conclusions drawn empirically by Gomez et al.[9]

■ ASSOCIATED CONTENT

Supporting Information

Sample preparation, experimental conditions, statistics parameters used in DQ NMR analysis, WAXD patterns, CPMAS NMR spectra, and CODEX best-fit parameters. This material is available free of charge via the Internet at http://pubs.acs.org.

■ AUTHOR INFORMATION

Corresponding Author

*E-mail: miyoshi@uakron.edu.

Notes

The authors declare no competing financial interest.

■ ACKNOWLEDGMENTS

This work was financially supported by the National Science Foundation (Grant DMR-1105829 and 1408855) and startup funds from the UA. We are thankful to Dr. Yamamoto for kindly providing the atomic coordinates of the calculated mesophase of *i*PP.

■ REFERENCES

(1) Coccorullo, I.; Pantani, R.; Titomanlio, G. *Polymer* **2003**, *44*, 307−318.
(2) Natta, G.; Corradini, P. *Nuovo Cimento* **1960**, *15*, 40−51.
(3) Allegra, G.; Meille, S. *Adv. Polym. Sci.* **2005**, *191*, 87−135.
(4) Caldas, V.; Brown, G. R.; Nohr, R. S.; MacDonald, J. G.; Raboin, L. E. *Polymer* **1994**, *35*, 899−907.
(5) Gailey, J. A.; Ralston, R. H. *Polym. Eng. Sci.* **1964**, *4*, 29−33.
(6) Wunderlich, B.; Möller, M.; Grebowicz, J.; Baur, H. *Conformational Motion and Disorder in Low and High Molecular Mass Crystals*; Advances in Polymer Science; Springer Verlag: New York, 1988; Vol. *87*.
(7) Corradini, P.; Petraccone, V.; De Rosa, C.; Guerra, G. *Macromolecules* **1986**, *19*, 2699−2703.
(8) Corradini, P.; De Rosa, C.; Guerra, G.; Petraccone, V. *Polym. Commun.* **1989**, *30*, 281−285.
(9) Gomez, M. A.; Tanaka, H.; Tonelli, A. E. *Polymer* **1987**, *28*, 2227−2232.
(10) Asakura, T.; Konakazawa, T.; Demura, M.; Ito, T.; Maruhashi, Y. *Polymer* **1996**, *37*, 1965−1973.
(11) Schmidt-Rohr, K.; Hu, W.; Zumbulyadis, N. *Science* **1998**, *280*, 714−717.
(12) Singh, M.; Schaefer, J. *J. Am. Chem. Soc.* **2011**, *133*, 2626−2631.
(13) Miyoshi, T.; Hu, W.; Hagihara, H. *Macromolecules* **2007**, *40*, 6789−6792.
(14) Fortier-McGill, B.; Toader, V.; Reven, L. *Macromolecules* **2012**, *45*, 6015−6026.
(15) Miyoshi, T.; Takegoshi, K.; Terao, T. *Macromolecules* **1999**, *32*, 8914−8917.
(16) Schmidt-Rohr, K.; Spiess, H. W. *Multidimensional Solid-State NMR and Polymers*; Elsevier: New York, 1994.
(17) Hong, Y.; Miyoshi, T. *ACS Macro Lett.* **2013**, *2*, 501−505.
(18) Hong, Y.; Miyoshi, T. *ACS Macro Lett.* **2014**, *3*, 556−559.
(19) Li, Z.; Miyoshi, T.; Sen, M. K.; Koga, T.; Otsubo, A.; Kamimura, A. *Macromolecules* **2013**, *46*, 6507−6519.
(20) DeAzevedo, E. R.; Hu, W.-G.; Bonagamba, T. J.; Schmidt-Rohr, K. *J. Am. Chem. Soc.* **1999**, *121*, 8411−8412.
(21) Mencik, Z. *J. Macromol. Sci., Part B: Phys.* **1972**, *6*, 101−115.
(22) Dorset, D. L.; McCourt, M. P.; Kopp, S.; Schumacher, M.; Okihara, T.; Lotz, B. *Polymer* **1998**, *39*, 6331−6337.
(23) Miyoshi, T.; Pascui, O.; Reichert, D. *Macromolecules* **2004**, *37*, 6460−6471.
(24) Miyoshi, T.; Mamun, A.; Reichert, D. *Macromolecules* **2010**, *43*, 3986−3989.
(25) Yamamoto, T. *Macromolecules* **2014**, *47*, 3192−3202.

■ NOTE ADDED AFTER ASAP PUBLICATION

This paper was published ASAP on January 9, 2015. First author's name was corrected. The revised paper was reposted on January 14, 2015.

DOI: 10.1021/mz5007969
ACS Macro Lett. 2015, 4, 143−146